Cis-Autophosphorylation of Juxtamembrane Tyrosines in the Insulin Receptor Kinase Domain†

Aaron Darius Cann and Ronald A. Kohanski*

Department of Biochemistry, Box 1020, The Mount Sinai School of Medicine, 1 Gustave L. Levy Place, New York, New York 10029

Received January 24, 1997; Revised Manuscript Received April 18, 1997⊗

ABSTRACT: Receptor tyrosine kinases undergo ligand-induced dimerization that promotes kinase domain *trans*-autophosphorylation. However, the kinase domains of the insulin receptor are effectively dimerized because of the covalent $\alpha_2\beta_2$ holomeric structure. This fact has made it difficult to determine the molecular mechanism of intraholomeric autophosphorylation, but there is evidence for both *cis*- and *trans*-autophosphorylation in the absence and presence of insulin. Here, using the cytoplasmic kinase domain (CKD) of the human insulin receptor, we demonstrate that autophosphorylation in the juxtamembrane (JM) subdomain follows a *cis*-reaction pathway. JM autophosphorylation was independent of CKD concentration over the range 6 nM−3 μM and was characterized kinetically: Half-saturation (K^{ATP}) was observed at 75 μM ATP [5 mM $Mn(CH_3CO_2)_2$] with a maximal rate of 0.24 mol of PO_4 (mol of CKD)$^{-1}$ min^{-1}. Pairwise substitutions of Phe for Tyr in the other two autophosphorylation subdomains, generated by site-directed mutagenesis, altered the kinetics of JM autophosphorylation but did not change the pathway from a *cis*-reaction. $Tyr^{1328,1334}$ to Phe (in the carboxy-terminal subdomain) yielded <2-fold increase in the efficiency of JM autophosphorylation, whereas $Tyr^{1162,1163}$ to Phe (in the activation loop subdomain) yielded ≈38-fold increased efficiency of JM autophosphorylation, due predominantly to a 23-fold decreased K^{ATP}. These findings demonstrate basal state binding of ATP to the CKD leading to *cis*-autophosphorylation and novel basal state regulatory interactions among the subdomains of the insulin receptor kinase. On the basis of these results and the crystal structure of the conserved catalytic core of this kinase [Hubbard, S. R., *et al*. (1994) *Nature 372,* 746], a model is proposed which reconciles the JM *cis*-reaction and the activation loop *cis*-inhibition/*trans*-reaction with the complex kinetics of insulin receptor autophosphorylation [Kohanski, R. A. (1993) *Biochemistry 32,* 5766].

Insulin binding to its receptor tyrosine kinase (RTK)[1] induces autophosphorylation, which leads to kinase activation and to increased phosphorylation of substrate proteins [reviewed in White and Kahn (1994)]. Autophosphorylation can occur at seven tyrosines in the insulin receptor (IR), which has a disulfide-bonded heterotetrameric structure composed of two insulin-binding α-subunits and two transmembrane, kinase-bearing β-subunits. These sites are present in three clusters in the intracellular region of the β-subunit: the juxtamembrane (JM), activation loop (AL), and carboxy-terminal (CT) subdomains of the receptor's β-subunit.[2] The AL tyrosines Y^{1158}, Y^{1162}, and Y^{1163} are regarded as the autophosphorylation sites primarily responsible for activation of substrate phosphorylation (Cherqui *et al*., 1990; Ellis *et al*., 1986; Murakami & Rosen, 1991; Zhang *et al*., 1991). Biological roles of autophosphorylation at the CT tyrosines Y^{1328} and Y^{1334} are not as well defined, but they do not appear to play a role in kinase activation or receptor internalization (Backer *et al*., 1992; Baron *et al*., 1991). Autophosphorylation in the JM subdomain at Y^{965} and Y^{972} may function in receptor internalization (Kaburagi *et al*., 1993; Rajagopolan *et al.*, 1991) and/or in the recruitment of substrates bearing PTB domains, such as IRS-1 or Shc (Eck *et al*., 1996; Isakoff *et al*., 1996). Although direct evidence for JM autophosphorylation has been obtained only recently (Feener *et al*., 1993; Kohanski, 1993b), autophosphorylation in the JM subdomain had been inferred earlier from mutagenesis in the JM subdomain leading to loss of IRS-1 phosphorylation (Backer *et al*., 1991, 1992; White *et al*., 1988). The three clusters of autophosphorylation sites in the insulin receptor thus play distinct but functionally coordinated roles in insulin signal transduction.

While the AL and JM sites are functionally linked—the former for increasing catalytic turnovers and the latter for recruiting signaling molecules for phosphorylation—they are not linked either in their abundance of autophosphorylation *in vivo* or in their autophosphorylation kinetics *in vitro*. Insulin-stimulated receptor autophosphorylation, either *in vivo* or *in vitro*, occurs primarily in the AL and CT subdomains. Despite its importance for substrate recruitment

† Supported by Grant DK50074 from the National Institutes of Health.

* To whom correspondence should be addressed. Phone: (212)-241-6897. Fax: (212)-996-7214. E-mail: kohanski@smtplink.mssm.edu.

⊗ Abstract published in *Advance ACS Abstracts,* June 15, 1997.

[1] Abbreviations: AL, activation loop; cAPK, cyclic AMP dependent protein kinase; CKD, cytoplasmic kinase domain (of the human insulin receptor); CT, carboxy terminus; DTT, dithiothreitol; EDTA, ethylenediaminetetraacetic acid; HEPES, 4-(2-hydroxyethyl)-1-piperazineethanesulfonic acid; HPLC, high-performance liquid chromatography; IR, insulin receptor; IRS-1, insulin receptor substrate 1; JM, juxtamembrane; PTB, protein tyrosine binding domain; RTK, receptor tyrosine kinase; SDS−PAGE, sodium dodecyl sulfate−polyacrylamide gel electrophoresis; Tris, tris(hydroxymethyl)aminomethane. To describe pairwise Tyr-to-Phe mutations in the kinase domains, ALY2F, $Y^{1162,3}$F; CTY2F, $Y^{1328,34}$F; and JMY2F, $Y^{965,72}$F were used.

[2] Residues in the insulin receptor and its fragments are numbered according to Ebina *et al*. (1985).

S0006-2960(97)00170-0 CCC: $14.00

in vivo, autophosphorylation in the JM subdomain is a very small fraction of insulin-stimulated net autophosphorylation (Flores-Riveros *et al*., 1989; Issad *et al*., 1991; Kohanski, 1993a,b; Tavare *et al*., 1988; Tavare & Denton, 1988; Tornqvist & Avruch, 1988; Tornqvist *et al*., 1987, 1988). A possible kinetic basis for these differences has been established, showing that the JM tyrosines react with a slower intrinsic rate than the AL and CT tyrosines (Kohanski, 1993a,b). Furthermore, there is evidence in the literature for the operation of two different molecular mechanisms of IR autophosphorylation: Both *intra*subunit and *inter*subunit autophosphorylations have been supported by analysis of $\alpha\beta$ half-receptors and of kinase active/inactive chimera [Shoelson *et al.* (1991) and Frattali *et al*. (1992), respectively]. It is therefore possible that the molecular basis underlying the different kinetics of subdomain autophosphorylation, and therefore the differences in JM *versus* AL plus CT phosphotyrosine levels, is a division between autophosphorylation pathways, respectively.

To distinguish effectively between *cis*- and *trans*-pathways in an autocatalytic reaction, Todhunter and Purich (1977) demonstrated that the enzyme concentration independence or dependence of the reaction suffices. However, this criterion cannot be effectively applied to the covalently linked holomeric IR. Therefore, we and others have analyzed autophosphorylation of the receptor's monomeric cytoplasmic kinase domain (CKD) as a model for the holomer: Using the CKD, evidence has been presented for either *cis*-autophosphorylation (Villalba *et al*., 1989), *trans*-autophosphorylation (Cobb *et al*., 1989; Wei *et al*., 1995), or both (Kohanski, 1993a). Furthermore, the recently solved crystal structure of the conserved catalytic core (Hubbard *et al*., 1994) was structurally consistent with the AL *trans*-autophosphorylation observed by Wei *et al*. (1995). That structure was solved from a kinase domain that, by N- and C-terminal truncations, lacked the JM and CT tyrosines and therefore left open the question of a *cis*-autophosphorylation mechanism for either of those two subdomains. In addition, there were several structural features identified that could explain why the basal state of the kinase had low catalytic activity and how initial autophosphorylation in the activation loop would have relieved those inhibitory constraints and permitted subsequent autophosphorylation or substrate phosphorylation events to occur. However, the *all-trans*-autophosphorylation model can accommodate a 2-to-1 ratio of JM-to-AL autophosphorylation, but it would not explain how, in the basal state holomeric insulin receptor, there could be a nearly 10-to-1 predominance of JM autophosphorylation over AL plus CT autophosphorylation (Kohanski, 1993a).

We have demonstrated previously that the complete CKD, from the first intracellular amino acid at R^{953} to the last residue at Ser^{1355}, is a good model for the holomeric IR's basal state (Kohanski & Schenker, 1991; Kohanski, 1993a,b). With this complete CKD, *cis*- *versus trans*-reaction within the JM subdomain was evaluated by determining the CKD concentration independence or dependence of autophosphorylation under conditions that allowed us to discriminate clearly among reactions in each subdomain. Computer-aided molecular modeling also suggested that, unlike Y^{1162}, the presence of Y^{972} in the active site of its own CKD molecule permits ATP binding and thus permits *cis*-autophosphorylation. By identifying a novel basal state conformer, these results expand our understanding of the molecular mechanisms of insulin receptor kinase autophosphorylation and activation.

EXPERIMENTAL PROCEDURES

Materials. Insulin-free radioimmunoassay-grade fraction V bovine serum albumin (BSA, catalog no. A-7888), grade V protamine chloride from salmon, and the disodium salt of ATP from equine muscle (catalog no. A-5394) were purchased from Sigma. [γ-^{32} P]ATP was synthesized from [^{32}P]-orthophosphate according to the method of Walseth and Johnson (1979) and purified (Palmer & Avruch, 1981). Other reagents were of at least reagent grade.

Construction and Expression of Mutant Kinases. A baculovirus encoding the wild-type (WT) CKD was a gift from the late Dr. Ora Rosen. This construct contained the complete intracellular portion of the β-subunit of the human insulin receptor, including residues 953−1355 (Villalba *et al*., 1989). Mutant forms of the CKD were identical to the WT CKD except for the following mutations: JMY2F CKD, $Y^{965}F$ and $Y^{972}F$; ALY2F CKD, $Y^{1162}F$ and $Y^{1163}F$; and CTY2F CKD, $Y^{1328}F$, $Y^{1334}F$ mutations. To ensure fidelity, all mutations and PCR products were verified by DNA sequencing. PCR was done with Vent polymerase (United States Biochemicals). Plasmids involved in the generation of these constructs are described below. Protein was expressed in a baculovirus expression system using recombinant baculoviruses constructed by recombination of baculovirus DNA with pVL1393 constructs using the BaculoGold kit (Pharmingen) according to manufacturers' instructions. Wild-type and mutant CKD were purified from baculovirus-infected Sf9 cells by the method of Villalba *et al.* (1989), with modifications: Anion-exchange chromatography was performed with a 1 × 10 cm DEAE 8HR column (Waters). The ammonium sulfate fractionation and the phenyl-Sepharose column were omitted. Size exclusion chromatography was done using a Superdex 75 16/60 or 26/60 column (Pharmacia). Enzyme concentrations were calculated from the absorbance at 280 nm, using an extinction coefficient of 40 200 M^{-1} cm^{-1} determined by the method of Hasselbacher *et al.* (1995) and Waxman *et al.* (1993; S. M. Bishop and R. A. Kohanski, unpublished observations). Purity of the CKD was assessed by SDS−PAGE using at least 2 μg of protein, and enzyme preparations used in this study were at least 95% pure.

Construction of the JMY2F Mutant. The construct pTZ19UIR (Whittaker *et al*., 1987), containing the human insulin receptor cDNA inserted into the MCS of pTZ19U, was a generous gift of Dr. J. Whittaker. The 1.7 kb *Bgl*I/*Bam*HI fragment from pTZ19UIR was ligated with 2.46 kB pSP72 (Promega) digested with *Kpn*I/*Bam*HI and two annealed oligonucleotides, 5′-CGCCACCATGAGAAA-GAGGCAGCCAGAT-3′ and 5′-CATGGCGGTGGTACT-CTTTCTCCGTCGGT-3′. The resulting construct, p72CKD, possessed a Kozak consensus sequence (CGCCACC) immediately upstream from an ATG methionine initiation codon and the in-frame nucleotide sequence encoding residues Arg^{953} to Ser^{1355} of the human insulin receptor. The mutations $Y^{965}F$ and $Y^{972}F$ were introduced using the overlap-extension polymerase chain reaction (PCR) method (Ho *et al*., 1989). PCR was done using p72CKD as template, with mutagenic oligonucleotide primers 5′-CTCAGGGTTTGAA-GAAGCGAAAAGCGGTC-3′ and 5′-CGCTTCTTCAAAC-

CCTGAGTTTCTCAGTGC-3′ and outside primers 5′-GACTCACTATAGGGAGACCG-3′ and 5′-CCATGCCG-AAGGATCCCTGC-3′. The final PCR product was inserted into the shuttle vector pXCKD, on *Eco*RI and *Xho*I sites. Details of pXCKD construction are described in Supporting Information. The resulting plasmid pXJMY2F encoded the same promoter and CKD sequence as p72CKD, except with the mutations described and a silent StuI site suppression encoded in pXCKD. The 1.6 kb *Eco*RI/*Pst*I insert from pXJMY2F was inserted into *Eco*RI/*Ps*tI digested baculovirus transfer vector pVL1393 (Pharmingen) to yield p93JMY2F, which was used for baculovirus generation.

Construction of the ALY2F Mutant. A cDNA containing the ALY2F mutations in pUIR19T (Poon *et al*., 1991) was a generous gift of Dr. Lu-Hai Wang. The *Stu*I/*Bst*XI insert from this construct, containing the mutation site, was subcloned into p72CKD. The *Eco*RI/*Pst*I insert from this was subcloned into pVL1393 to yield p93ALY2F, which was used for baculovirus generation.

Construction of the CTY2F Mutant. The CTY2F construct was constructed by a mutagenesis scheme similar to that used for the JMY2F construct. The mutagenic inner primers were 5′-AAGGGATGTGTTCCTCGAAGCTCCGCTTG-AAACC-3′ and 5′-CGAGGAACACATCCCTTTCACACA-CATGAACG-3′, the nonmutagenic outer primers were 5′-CCAGCTTTCCAGAGGTGTCG-3′ and 5′-GTTGCCCC-AAAGGAGCAGC-3′, and the template used for the PCR was pTZ19UIR. The PCR product was digested with *Avа*I and *Spe*I and ligated to the 0.9 and 3.6 kb *Avа*I/*Spe*I fragments from pXCKD in a three-part ligation. The resulting mutant CKD gene was moved into pVL1393 using *Eco*RI and *Pst*I sites and used for baculovirus generation.

Autophosphorylation Reactions. Autophosphorylation reactions were for 1 min in 50 mM HEPES, pH 7.0, containing 5 mM fresh manganese acetate (MnOAc), 0.1% bovine serum albumin (BSA, w/v), 1 mM dithiothreitol (DTT), 4% glycerol (v/v), and [γ-^{32} P]ATP at concentrations specified in the figure legends. Reactions (20−60 μL) were quenched by addition of 0.5 volume of 3× Laemmli sample buffer containing 6% sodium dodecyl sulfate (SDS, w/v), 60 mM EDTA, 20% glycerol, and 50 mM DTT in 18.9 mM Tris-HCl, pH 6.8, and analyzed by SDS−PAGE as described (Kohanski & Schenker, 1989). The stoichiometries resulting from autophosphorylation under various conditions were determined from Cherenkov counting of ^{32}P-labeled CKD excised from Coomassie blue-stained and dried gels. The specific radioactivity of [γ-^{32}P]ATP was determined in parallel for these measurements.

Two-Dimensional Phosphopeptide Mapping. Autophosphorylated ^{32}P-labeled CKD was isolated for proteolytic digestion as discussed previously (Kohanski & Schenker, 1989). Proteolysis was done for 16−24 h using 1 μg of endoproteinase Lys-C (Wako Chemicals) in 0.5 mL of 50 mM ammonium bicarbonate with a second addition of protease at 12−18 h. Gel fragments were recovered by centrifugation, and the supernatant was lyophilized in a Savant Speed-Vac. Samples were resuspeneded in water and relyophilized 6−7 times. Two-dimensional phosphopeptide mapping for determination of autophosphorylation sites was performed according to Boyle *et al*. (1991) with the following modifications: Samples were reconstituted in 5−15 μL of 20% acetic acid, and 1−5 μL was spotted onto 20 × 20 cm Kodak cellulose TLC plates (Eastman 13255). Electrophoresis at 16 °C in 20% acetic acid and 5% 1-butanol was for 1 h at 1000 V, with a 19 cm separation between electrodes. Ascending chromatography was done in butanol−pyridine−acetic acid−water (15:10:3:12, v/v). Radiolabeled phosphopeptides were visualized by autoradiography using Kodak XAR X-ray film.

RESULTS

Reaction Conditions for Juxtamembrane Autophosphorylation. To study the molecular mechanism of juxtamembrane autophosphorylation in WT and mutant CKDs, we utilized reaction conditions where these sites make the dominant contribution to net autophosphorylation. Previous kinetic studies had revealed that JM autophosphorylation was favored over AL or CT autophosphorylation by low ATP concentrations and short reaction times (Kohanski, 1993a). We therefore used 10 μM ATP in a 1 min autophosphorylation reaction. These conditions yielded low stoichiometries of autophosphorylation. Therefore, reactions were done at 1.4 μM CKD which still maintained the pseudo-first-order constraint of [ATP] >> [CKD] while maximizing the signal-to-noise ratio for radioisotope incorporation.

To show that JM autophosphorylation was predominant in WT, ALY2F, and CTY2F CKD under these reaction conditions, [^{32}P]phosphopeptide maps were generated (Figure 1A−C, respectively). In each of these three maps, ≥80% of net autophosphorylation was detected in one region of the map, designated "J" and shown by the following analyses to originate from autophosphorylation in the JM subdomain. A [^{32}P]phosphopeptide map generated from JMY2F lacked peptides in this region but still had the phosphopeptides observed in other regions of the map generated from WT CKD autophosphorylated to a high stoichiometry (Figure 1D *versus* 1E). The absence of the AL monophosphopeptide A1 from the JMY2F mutant autophosphorylated at higher ATP concentration and longer time (Figure 1D) reflects the greater extent of reaction under these conditions. Consistent with this finding, the bis- and trisphosphopeptides assigned to the AL subdomain were not detected in the map generated from autophosphorylated ALY2F although the monophosphopeptide A1 from this subdomain could be generated and was detected (Figure 1B); the AL trisphosphopeptide was not detected in a mutant with only a Tyr^{1158}-to-Trp mutation although the mono- and bisphosphopeptides could be generated and were found (not shown). Finally, no phosphopeptides in the region designated C (carboxy-terminal mono- and bisphosphopeptides) were detected in the map generated from autophosphorylated CTY2F (Figure 1C). The peptides from region J of the maps shown in Figure 1E (and maps similar to Figure 1A−C) were extracted and analyzed by reverse-phase HPLC as described previously (Kohanski, 1993b) and eluted as JM phosphopeptides (not shown). The variable migration of J-phosphopeptides in these analyses probably resulted from differences in the amounts of residual salts in the samples prior to electrophoresis. These observations demonstrate that region J of these maps is properly assigned to phosphopeptides derived from the JM subdomain of the CKD. This conclusion is similar to that of Engl *et al*. (1994) but differs from that of Tavare *et al*. (1991) in their respective analyses of tryptic [^{32}P]phosphopeptides from

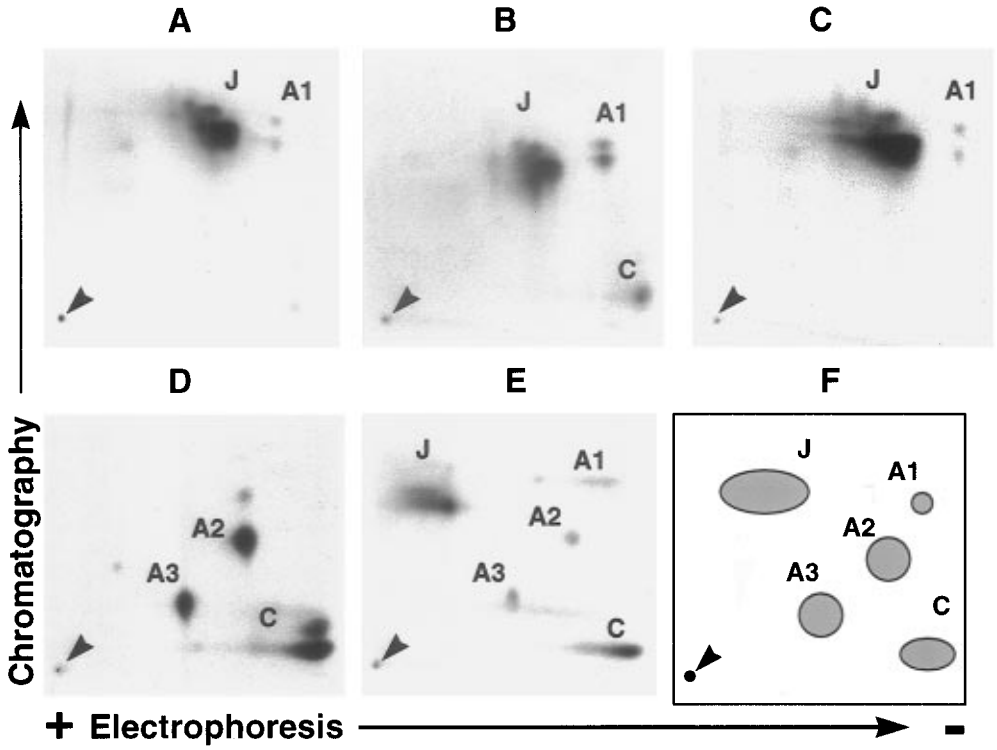

FIGURE 1: [^{32}P]Phosphopeptide maps from autophosphorylated WT and mutant CKD. Autoradiograms in panels A−E show the two dimensional [^{32}P]phosphopeptide maps generated by endoproteinase Lys-C digestion after autophosphorylation reactions of WT and mutant CKDs with [γ-^{32}P]ATP. All autoradiograms are oriented for the same directions of electrophoresis and chromatography, as indicated outside the panels. The sample application origin is marked on each panel with an arrowhead. One minute reactions at 10 μM [γ-^{32}P]ATP and 1.4 μM CKD were done with WT (A), ALY2F (B), or CTY2F (C). Twenty minute reactions at 500 μM [γ-^{32}P]ATP and 1.4 μM CKD were done with JMY2F (D) and WT (E). Autophosphorylation subdomain assignments were made for each [^{32}P]phosphopeptide, as described in the text and summarized in panel F: J, juxtamembrane; A1, A2, and A3, activation loop mono-, bis-, and trisphosphorylated; C, carboxy terminus. Autoradiogram exposure times in panels A−C were adjusted to give approximately equal saturation of the X-ray film for the J region. Further details are given in the text.

the insulin receptor. The assignments of these mapped [^{32}P]-phosphopeptides to the three subdomains of the insulin receptor, based on the above comparisons among maps generated from autophosphorylated WT CKD and selected Phe-for-Tyr substitutions, are summarized in Figure 1F.

CKD Concentration Independence of JM Autophosphorylation. Todhunter and Purich (1977) determined that the enzyme concentration dependence or *in*dependence of an autocatalytic reaction differentiates between inter- *versus* intramolecular reaction pathways, respectively, in this case, between *cis*- or *trans*-autophosphorylation of the CKD. In a *cis*-autophosphorylation reaction, formation of phosphorylated CKD should depend linearly on the concentration of CKD, so that the stoichiometry of autophosphorylation (mol of PO_4/mol of CKD) would be independent of CKD concentration. In contrast, a *trans*-autophosphorylation mechanism, where one kinase molecule phosphorylates another, requires kinetically significant interactions between kinase molecules. In this case autophosphorylation of CKD would have a second-order dependence on total CKD concentration. Therefore, in a *trans*-autophosphorylation reaction, the *stoichiometry* of autophosphorylation would increase linearly with increasing CKD concentration. Under the reaction conditions described in Figure 1A−C, ≥90% of the net autophosphorylation occurred in the JM subdomain. Thus, analysis of the stoichiometry of CKD autophosphorylation as a function of CKD concentration can differentiate between the two possible molecular mechanisms of JM autophosphorylation.

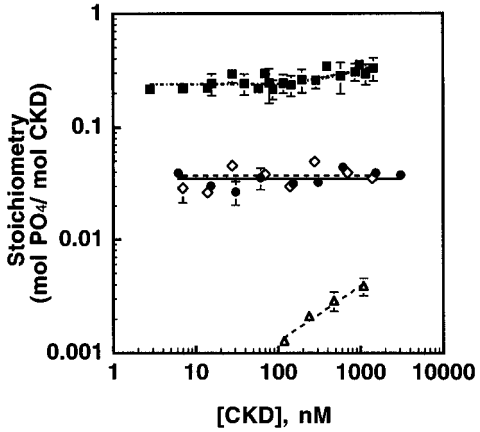

FIGURE 2: CKD concentration dependence of autophosphorylation at 10 μM ATP. The stoichiometry of net autophosphorylation of WT and mutant CKDs was measured over a range of CKD concentrations after 1min reactions at 10 μM [γ-^{32}P]ATP (specific radioactivity 10−27 cpm/nmol by Cherenkov counts). Data shown are the average of quadruplicate determinations, and the error bars show ±1 standard deviation. The CKDs were WT (●), ALY2F (■), CTY2F (◇), and JMY2F (△), at the concentrations indicated. Logarithmic scales have been used for both axes. Further details are given in the text.

The stoichiometries of autophosphorylation of WT CKD and three Tyr-to-Phe mutant CKDs were measured over broad ranges of CKD concentrations (Figure 2). These results show that autophosphorylation stoichiometries of the WT and CTY2F CKDs are each independent of enzyme concentration. The apparent reaction orders, as derived from these plots, are 1.04 ± 0.02 and 1.05 ± 0.03, respectively.

Within experimental error, net autophosphorylation in each of these kinases fits the criterion of concentration independence that establishes a *cis*-autophosphorylation reaction pathway. Together with results from the [^{32}P]phosphopeptide maps (Figure 1A,B), these findings demonstrate *cis*-autophosphorylation in the JM subdomain.

Net autophosphorylation of ALY2F CKD was independent of CKD concentration below 145 nM, with a reaction order of 1.03 ± 0.02. However, net autophosphorylation shows a dependence on concentration over the range 290−1500 nM kinase, yielding a reaction order of 1.13 ± 0.04. This greater-than-first order-in-CKD dependence for net autophosphorylation of ALY2F CKD represents a greater contribution from *trans*-autophosphorylation of the remaining AL tyrosine (Y^{1158})and the CT tyrosines.[3]

Autophosphorylation of the JMY2F CKD, in contrast, was highly enzyme concentration dependent, with an apparent reaction order of 1.5 ± 0.05 (Figure 2). This observation is consistent with significant *trans*-autophosphorylation in the AL and CT tyrosines, which are still present in this CKD. The stoichiometry of autophosphorylation in JMY2F CKD was ≤10% that of the WT, even at 1.1 μM enzyme (Figure 2). This result fits with reaction conditions that promoted ≥90% of net autophosphorylation in the JM subdomain, autophosphorylation sites that the JMY2F CKD does not possess.

In the WT CKD and two variants of the CKD, JM autophosphorylation was clearly independent of CKD concentration and therefore followed a *cis*-autophosphorylation pathway. Where autophosphorylation was restricted by mutagenesis to the AL and/or CT tyrosines, the reaction showed more second-order characteristics, consistent with *trans*-autophosphorylation in these subdomains. Further experimental evidence in support of this conclusion is presented below.

ATP Concentration Dependence of Juxtamembrane Autophosphorylation. Over the concentration range where autophosphorylation of ALY2F CKD was kinase concentration independent, ALY2F CKD incorporated 6-fold more PO_4 from ATP than the WT or CTY2F (Figure 2). The average stoichiometries were 0.23 ± 0.02, 0.04 ± 0.01, and 0.04 ± 0.01 mol of PO_4/mol of CKD, respectively. Importantly, this increased level of autophosphorylation was still due to *cis*-reactions in the JM subdomain. This increased stoichiometry of autophosphorylation could arise from changes in kinetic parameters affected by the $Y^{1162,3}$-to-$F^{1162,3}$ amino acid replacements. Since the only variable substrate in the *cis*-reaction of JM tyrosines is ATP, we compared the ATP dependence for autophosphorylation of the WT, ALY2F, and CTY2F CKDs (Figure 3), which yielded the kinetic parameters summarized in Table 1.

[3] There was proportionally less JM autophosphorylation in the ALY2F CKD than in either the WT or CTY2F CKD (Figure 1B *versus* 1A and 1C; ~80% of net autophosphorylation was in the JM subdomain in ALY2F measured at 1.4 μM kinase, compared to ≥90% in the WT and CTY2F CKDs). These results are consistent with a *cis*-reaction pathway for autophosphorylation where the JM subdomain predominated (at concentrations of ALY2F ≤145 nM, [^{32}P]phosphopeptide maps not shown) but also with a *trans*-reaction pathway for CT and/or AL autophosphorylation. Therefore, in the ALY2F CKD, we observed a change from concentration independence to concentration dependence that indicates a change from *cis*- to a mixture of *cis*- and *trans*-autophosphorylation mechanisms.

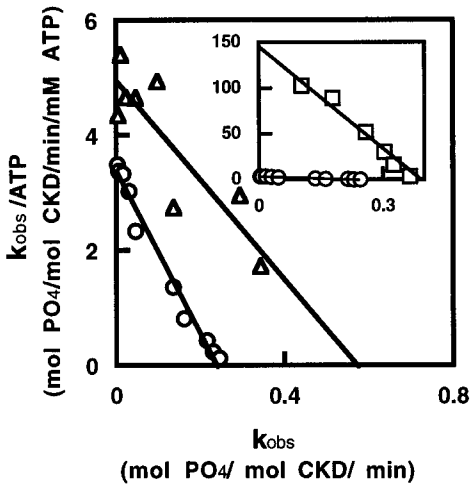

FIGURE 3: ATP dependence for juxtamembrane autophosphorylation. The apparent rate of reaction for JM autophosphorylation (k_{obs}) was determined from duplicate 1 min reactions of WT and mutant CKDs over a range of [γ-^{32}P]ATP concentrations at 0.01% BSA (w/v). The data are shown as Eadie−Scatchard plots for 100 nM WT CKD (○), 120 nM CTY2F CKD (△), and 120 nM ALY2F CKD (□; inset, using a different scale but with data from WT CKD replotted for comparison). The concentration ranges of [γ-^{32}P]ATP were 1−2000 μM for WT CKD and 1−200 μM for CTY2F and ALY2F CKD. Further details of the assay are given under Experimental Procedures.

Table 1: ATP Dependence of Juxtamembrane Autophosphorylation[a]

enzyme	K^{ATP} (μM)	k_{obs} (mol mol^{-1} min^{-1})	k_{obs}/K^{ATP} ($\times 10^{-3}$ min^{-1} M^{-1})	$\Delta\Delta G^b$ (kcal/mol)
WT	75 ± 3	0.24 ± 0.02	3.2	N/A
CTY2F	120 ± 16	0.59 ± 0.06	4.9	−0.25
ALY2F	3.2 ± 0.3	0.39 ± 0.10	121.0	−2.2

[a] The data from the Eadie−Scatchard plots in Figure 3 were analyzed by linear regression to extract an apparent first-order rate constant for the *cis*-reaction of JM autophosphoryation (k_{obs} from the *x*-axis intercept) and the apparent dissociation constant for ATP binding (K^{ATP} from the negative of 1/slope of each plot). Errors shown are ±1 standard deviation. [b] Calculated from $\Delta\Delta G = -RT \ln\{(k_{obs}/K^{ATP})_{mut}/(k_{obs}/K^{ATP})_{WT}\}$.

Using the constants in Table 1, we calculated autophosphorylation stoichiometries for the reaction conditions described for Figure 2. These calculated values of mol of PO_4/mol of CKD agreed well with the measured stoichiometries: 0.03 *versus* 0.04 for WT CKD, 0.04 *versus* 0.04 for CTY2F CKD, and 0.30 *versus* 0.23 for ALY2F CKD (≤145 nM kinase). The kinetic parameters for JM autophosphorylation in Table 1 yield predictions for the stoichiometries of JM autophosphorylation that fit well with the observed values (Figure 2). Importantly, these observations confirm that the increased stoichiometry of JM autophosphorylation in the ALY2F CKD at concentrations ≤145 nM kinase resulted from a more efficient reaction at JM tyrosines and not because of a switch to *trans*-autophosphorylation mechanisms.

Trans-Autophosphorylation of the Activation Loop and Carboxy-Terminal Tyrosines. We have presented compelling evidence for *cis*-autophosphorylation in the JM subdomain of the IR CKD, including Y^{965} and Y^{972}. Y^{965} of the IR is conserved only among insulin, insulin-like growth factor I, and insulin receptor-related receptor tyrosine kinases, and Y^{972} of the IR is conserved among these three RTKs and also TrkA, TrkB, and leukocyte tyrosine kinase (Hanks *et al.*, 1988). However, it is generally accepted that kinase

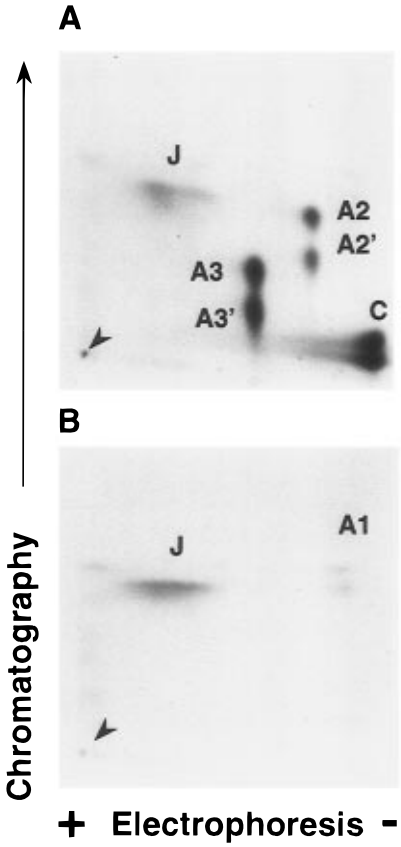

FIGURE 4: [^{32}P]Phosphopeptide maps from WT CKD autophosphorylated at 500 μM [γ-^{32}P]ATP. Autoradiograms showing the two-dimensional [^{32}P]phosphopeptide maps generated by endoproteinase Lys-C digestion after 1 min autophosphorylation reactions of 0.7 μM WT CKD at 500 μM [γ-^{32}P]ATP in the presence (panel A) versus the absence (panel B) of protamine chloride (30 μg/mL). Both autoradiograms are oriented for the same directions of electrophoresis and chromatography, as indicated outside the panels. The sample application origin is marked on each panel with an arrowhead. The autophosphorylation subdomain assignments are the same as shown in Figure 1. The doublets marked A2′ and A3′ originate from the same phosphopeptides as A2 and A3, respectively; they are artifacts that arose during chromatography, as described under Experimental Procedures. A_1′ and C′ are not marked for simplicity.

domains of RTKs autophosphorylate *in trans* (van der Greer, 1994). Crystallographic data support *trans*-autophosphorylation in the activation loop tyrosines residing within the conserved catalytic core of the insulin receptor and fibroblast growth factor receptor kinase domains (Hubbard *et al*., 1994; Mohammadi *et al*., 1996). Therefore, a control for the observed *cis*-autophosphorylation of JM tyrosines would be evidence for *trans*-autophosphorylation of AL tyrosines. On the basis of previous kinetic and autophosphorylation site mapping studies (Kohanski, 1993a,b), if the AL tyrosines react by a *trans*-pathway, then the CT tyrosines are also expected to react by a *trans*-pathway. Reaction at the AL and CT tyrosines is favored by high ATP concentrations and the presence of a stimulator of autophosphorylation (Kohanski, 1989, 1993b). The stimulator could be insulin or polycations for the native receptor (Kohanski, 1989; Morrison *et al*., 1988; Rosen & Lebwohl, 1988; Sacks & MacDonald, 1988) and polycations and some cationic substrates for the native receptor and the CKD (Kohanski & Schenker, 1991; Cobb *et al*., 1989). For the experiments described below, protamine chloride was used, since Cobb *et al*. (1989) had shown in the presence of protamine a CKD concentration

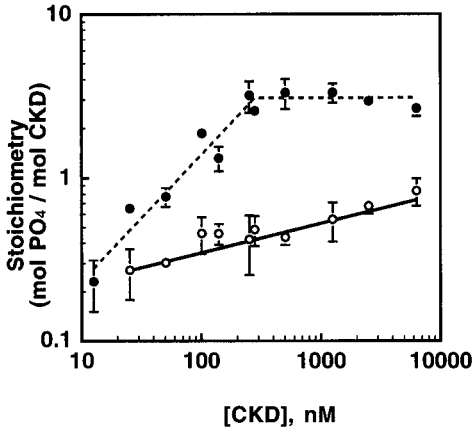

FIGURE 5: Enzyme concentration dependence of AL and CT autophosphorylation. The stoichiometry of autophosphorylation of WT CKD was measured under reaction conditions that favored the AL and CT subdomains. Reactions were done for 1 min in the presence (●) versus the absence (○) of protamine chloride (30 μg/mL) at 500 μM [γ-^{32}P]ATP, at the indicated concentrations of CKD. Data are expressed on a log-log plot and represent the averages of triplicate determinations with the error bars representing ±1 standard deviation. Additional details are provided in the text.

dependence for net autophosphorylation, which is the essential evidence for a *trans*-autophosphorylation mechanism.

At 0.5 mM ATP and in the presence of protamine chloride, >90% of net autophosphorylation occurred in the AL and CT tyrosines, with the bis- and trisphosphorylated (but not the monophosphorylated) AL peptides and the monophosphorylated CT peptides predominating (Figure 4A). In contrast, without protamine but also at 0.5 mM ATP, ~80% of net autophosphorylation was in the JM subdomain and ~20% of net autophosphorylation was in the AL subdomain; the AL monophosphopeptide but not the bis- or trisphosphopeptides was observed (Figure 4B). On the basis of these observations, measurement of net autophosphorylation over a concentration range of CKD, from reactions at 0.5 mM ATP in the presence of protamine chloride, will report primarily on the reaction order of AL and CT autophosphorylation.

Autophosphorylation of WT CKD in the presence of protamine demonstrated an apparent reaction order of 1.8 ± 0.1, at concentrations of CKD below 280 nM (Figure 5). This is consistent with autophosphorylation dominated by *trans*-reactions; *i.e.*, autophosphorylation in the AL and CT subdomains (Figure 4A). The apparent leveling off of the reaction above 280 nM CKD represents a mixture of effects: The ratio of polycation to CKD becomes suboptimal for stimulation, and the extent of net reaction begins to approach its end point. Autophosphorylation of WT CKD without protamine present yielded an apparent reaction order of 1.20 ± 0.03. This reaction order and the results of Figure 4B suggest that autophosphorylation under these conditions is a mixture of *cis*- and *trans*-reaction pathways in the JM and AL plus CT subdomains, respectively. These results show that the assays employed here can report intermolecular autophosphorylation. Therefore, the intramolecular JM autophosphorylation in WT, ALY2F, and CTY2F CKDs inferred from the data in Figure 2 is the product of an intrinsic molecular mechanism and does not result from a technical difficulty or systematic error obscuring *trans*-reactions. Taken together, we have used reaction conditions that favor either JM autophosphorylation or AL and CT

autophosphorylation of the insulin receptor's catalytic domain and have demonstrated that these proceed respectively by *cis*- and *trans*-reaction mechanisms.

DISCUSSION

The complete cytoplasmic kinase domain purified from baculovirus-infected Sf9 insect cells is a good model for studying regulation of insulin receptor autophosphorylation. Previous work has shown it to be functionally analogous to the basal state of the native insulin receptor (Kohanski, 1993a,b; Kohanski & Schenker, 1991): Specifically, the CKD displayed ATP dependencies and subdomain reactivities for autophosphorylation similar to those observed with intact insulin receptor in the absence of insulin. Furthermore, the CKD could be stimulated to yield ATP dependencies and subdomain reactivities similar to those of insulin-stimulated native receptor. To understand the molecular mechanisms of autophosphorylation, in this study we took advantage of the monomeric nature of the CKD to apply the concentration dependence criteria described by Todhunter and Purich (1977). We demonstrated conclusively *cis*-autophosphorylation in the CKD under reaction conditions that favored reaction in the JM subdomain. By using site-directed mutagenesis to substitute Phe for Tyr at known autophosphorylation sites, we provided additional strong evidence that *cis*-autophosphorylation was specific to the JM subdomain. Similarly, deviations from *cis*-autophosphorylation resulted from increasing *trans*-autophosphorylation within the AL and CT subdomains.

Evidence for at least partial *cis*-subunit autophosphorylation in holomeric insulin receptor or in $\alpha\beta$ half-receptors has been described (Frattali *et al.*, 1992; Böni-Schnetzler *et al*., 1986; Sweet *et al.*, 1987; Wilden *et al.*, 1989a,b; Shoelson *et al*., 1991). However, identities of the autophosphorylation site(s) reacting by either the *cis*- or *trans*-pathways were not reported. Two different "kinetic pathways" for autophosphorylation in the insulin receptor were identified in previous work (Kohanski, 1993a). Reaction of JM tyrosines was favored by low ATP concentrations and the absence of any stimulators and was more characteristic of basal state (unstimulated) autophosphorylation. Reactions of AL and CT tyrosines were favored by high ATP concentrations and the presence of stimulating agents (insulin or polycations) and were more characteristic of the activated state in both the CKD and the native receptor. As described here, the underlying molecular basis for these differences in kinetic parameters is a difference in *cis*- as opposed to *trans*-autophosphorylation mechanisms. These findings also account for the *cis*- and *trans*-autophosphorylations reported by other laboratories.

In contrast to our present findings, amino-terminally truncated versions of the CKD appeared to lack *cis*-autophosphorylation pathways (Cobb *et al*., 1989; Wei *et al*., 1995). The CKD employed by Wei *et al*. (1995) and crystallized by Hubbard *et al*. (1994) contained only the activation loop autophosphorylation sites, so the lack of *cis*-autophosphorylation reflected the absence of the JM sites that proceed *via* this pathway. That crystal structure showed a "basal state" conformer that was inactive due to orientation of the two lobes of the kinase and was "*cis*-inhibited" by structural features of the activation loop that precluded peptide or ATP binding. Important to our understanding of the basal state, and therefore to structural and thermodynamic barriers to activation, is that our findings demonstrated a basal state conformer that does bind ATP **and** catalyzes a *cis*-autophosphorylation. To demonstrate the compatibility of these conclusions with known crystal structures of protein kinases, we developed a structural model illustrating *cis*-autophosphorylation of Y^{972} of the JM subdomain. It was based on the proposal of Taylor *et al*. (1993) that the cyclic AMP dependent protein kinase (cAPK) is a paradigm for the catalytically active complex of most protein kinases. The ternary complex of cAPK with ATP and a peptide inhibitor (Knighton *et al*., 1991; Zheng *et al*., 1993) therefore served as the three-dimensional template for the model structure of *cis*-autophosphorylation. Many of the conclusions reached by Hubbard *et al*. (1994) used a comparison of the IR kinase domain with the cAPK, and we have followed most of their logic in making changes in lobe orientations and positioning of significant catalytic residues.[4]

The resulting model structure is shown in Figure 6. To the extent that the structure presented by Hubbard *et al*. (1994) is evidence against a *cis*-reaction for Y^{1162}, the model developed here is compatible with *cis*-autophosphorylation of Y^{972}. It illustrates a conformer of this kinase that is derived from evidence presented in this report for an *intra*molecular reaction mechanism within at the JM subdomain.

There are several important conclusions that can be drawn from this model and the observations made in this study. These shed new light on basal state conformations accessible to the insulin receptor's kinase domain but which remain consistent with principles established from the crystal structure. *First*, the observation that *cis*-autophosphorylation

[4] The cAPK−ATP−PKI structure appears to represent a catalytically competent conformer shared by all protein kinases, expect for the absence of the phosphoryl acceptor hydroxyl group on PKI (Taylor *et al*., 1993). Crystallographic data were obtained from the Brookhaven National Laboratory Protein Data Bank files 1IRK (for the catalytic core of the CKD; Hubbard *et al*., 1994) and 1ATP (for the ternary complex of cAPK; Zheng *et al*., 1993). To generate a structure compatible with ATP binding and phosphoryl transfer, each lobe of the CKD was superimposed separately onto the corresponding lobe of the cAPK ternary complex crystal structure (Taylor *et al*., 1993; Zheng *et al.*, 1993). Residues 1149−1161 and 1167−1172 of the IR were reoriented to overlap residues 182−202 of cAPK. This relocation of the analogous segments of the IR activation loop (without five amino acids that are not conserved) would permit ATP binding by placing F^{1151} in the region near H^{1130} and M^{1051}, as proposed by Hubbard *et al*. (1994). The five amino acid insert of the activation loop of IR (Y^{1162}−G^{1166}) was added between D^{1161} and G^{1167}, followed by bond angle and length normalization and energy minimization. ATP was inserted into its binding site, again by homology with its position in the cAPK ternary complex crystal structure, although the phosphate chain had to be shifted slightly to accommodate small differences between orientations of the glycine-rich loops of cAPK and the IR (G^{1003}−G^{1008} in IR). The structure developed so far is a conformer capable of phosphoryl transfer, except for the absence of a phosphoryl acceptor. To complete a model structure for *cis*-autophosphorylation, the amino acids $EY^{972}L$ of the JM subdomain were placed in the same positions as $DY^{1162}Y$ of the original IR crystal structure This directed the hydroxyl group of Y^{972} toward the catalytic base D^{1132} and placed it near the γ-phosphoryl group of ATP. Residues 974−984 were inserted as an extended chain across the surface of the small lobe to L^{973}, from the first spatially defined residue in the crystal structure, V^{985}. The side chains of two residues in helix C (R^{1030} and N^{1046}) were repositioned to accommodate the new sequence from the JM subdomain. Finally, we did an energy minimization of the repositioned activation loop and the sequence added from the JM subdomain. The configurations of the backbone and side chains are compatible with the limits of $\phi-\psi$ angles and steric considerations.

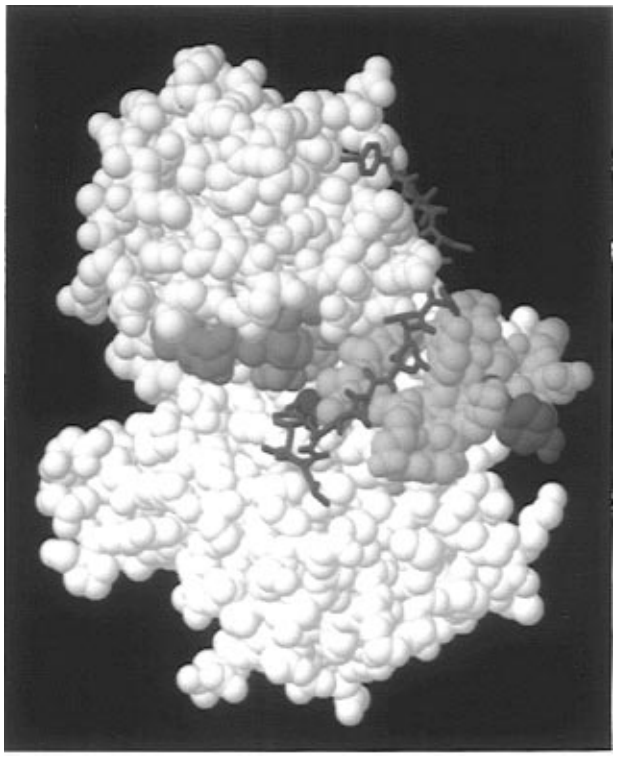

FIGURE 6: Molecular model for juxtamembrane *cis*-autophosphorylation. A possible basal state conformer allowing JM *cis*-autophosphorylation of Y^{972} was constructed on the basis of the crystal structures of the IR CKD and the ternary complex of cAPK, as described in the text. The space-filling model shows the small lobe in yellow, the large lobe in white, the activation loop in cyan with Y^{1162} in red and F^{1151} in gray, the catalytic base D^{1132} in dark blue, the bound ATP in magenta, $G^{1003}-G^{1008}$ of the Gly-rich ATP binding loop in green, and the amino acid sequence $E^{971}-Y^{984}$ from the JM subdomain as a stick drawing in red. The phenolic hydroxyl of Y^{972} is oriented toward the presumed catalytic base, D^{1132}. The position of Y^{1162} is not compatible with the hydrogen bond contacts proposed by Hubbard *et al*. (1994) for the activated state, following autophosphorylation of that AL tyrosine. The model was drawn using Quanta, and the figure was prepared using RASMOL. Further details of the model and its implications are discussed in the text.

of JM tyrosines display saturation with increasing ATP concentration indicates that a Michaelis complex was formed during the reaction and therefore an enzyme-catalyzed reaction had occurred. This means that JM tyrosines and ATP interacted at a catalytic center. This leads directly to the *second* conclusion: The fact of *cis*-autophosphorylation of JM tyrosines in itself demonstrates a basal state conformer capable of binding ATP in solution. In contrast, ATP binding was excluded in the crystallized conformer by the activation loop. *Third*, the rate constant for JM *cis*-autophosphorylation indicates a slow phosphoryl transfer reaction in the basal state. The molecular basis for this is presently not clear. There could be a rate-limiting release of the JM subdomain from the active site after *cis*-autophosphorylation. Alternatively, there could be competition among autophosphorylation subdomains for the active site. Because the Tyr-to-Phe mutations in the AL and CT subdomains yielded approximately the same modest 2−3-fold increase in k_{obs} (Table 1), this could suggest that CT tyrosines can also be in the active site, but in a state that does not bind ATP. This proposal fits the observation that AL and CT autophosphorylations have similar kinetic parameters (Kohanski, 1993a). *Fourth*, the Tyr-to-Phe mutations in the AL increased the catalytic efficiency of JM autophosphorylation nearly 40-fold (k^{obs}/K^{ATP} in Table 1) whereas catalytic efficiency was not altered significantly by the Tyr-to-Phe changes in the CT subdomain. These findings are strikingly supportive of the unusual feature observed in the crystal structure, which was that the activation loop inhibited ATP binding in addition to blocking peptide substrate binding (Hubbard *et al*., 1994). The effective free energy difference ($\Delta\Delta G$, Table 1) of ~2 kcal/mol reflected by the increased catalytic efficiency of the ALY2F is equivalent to the free energy typically associated with 1−2 hydrogen bonds. Hydrogen bonds involving the side chains of Y^{1162} and Y^{1163} were described by Hubbard *et al*. (1994), but they are absent in ALY2F.

In comparing the model shown in Figure 6 with the crystal structure of the conserved core of the kinase, we conclude the following. *First*, there are at least two basal state conformers which are both *cis*-inhibited with respect to peptide substrate phosphorylation. *Second*, the AL and JM subdomain tyrosines are mutually inhibitory because they are mutually exclusive. The first implication would further suggest that JM autophosphorylation should yield some activation of peptide substrate phosphorylation, which is the case (A. D. Cann and R. A. Kohanski, manuscript in preparation). On the basis of the second implication and the four conclusions listed above, the major autoinhibitory affect of the AL would be on ATP binding; therefore, disrupting specific interactions that stabilize the activation loop *cis*-inhibited conformer would enhance *cis*-autophosphorylation in the juxtamembrane subdomain by altering the ATP dependence for that reaction. This was observed with the ALY2F mutant described above and is evidence for unexpected interactions among the subdomains involved in autophosphorylation. Therefore, by determining the subdomain specificity of *cis*- and *trans*-reactions, these studies using the complete kinase domain and selected mutants have revealed additional and novel mechanisms for regulation of insulin receptor autophosphorylation.

ACKNOWLEDGMENT

We thank Dr. J. Whittaker for providing the plasmid pTZ19UIR, Dr. L.-H. Wang for providing a cDNA including the mutations used in the ALY2F CKD, and Dr. H. Weinstein for access to the Silicon Graphics workstations in the Molecular Modeling Core Facility at Mount Sinai School of Medicine.

SUPPORTING INFORMATION AVAILABLE

A description of the construction of the cytoplasmic kinase domain cassette vector pXCKD and one figure showing a diagram of the pXCKD-based constructs (4 pages). Ordering information is given on any current masthead page.

REFERENCES

Backer, J. M., Schroeder, G. G., Cahill, D. A., Ullrich, A., Siddle, K., & White, M. F. (1991) *Biochemistry 30*, 6366−6372.

Backer, J. M., Schroeder, G. G., Kahn, C. R., Myers, M. G., Wilden, P. A., Cahill, D. A., & White, M. F. (1992) *J. Biol. Chem. 267*, 1367−1374.

Baron, V., Gautier, N., Kaliman, P., Dolais-Kitabgi, J., & Van Obberghen, E. (1991) *Biochemistry 30*, 9365−9370.

Boni-Schnetzler, M., Rubin, J. B., & Pilch, P. F. (1986) *J Biol. Chem. 261*, 15281−15287.

Boyle, W. J., van der Greer, P., & Hunter, T. (1991) *Methods Enzymol. 201*, 110−152.
Cherqui, G., Reynet, C., Caron, M., Melin, B., Wicek, D., Clauser, E., Capeau, J., & Picard, J. (1990) *J. Biol. Chem. 265*, 21254−21261.
Cobb, M. H., Sang, B.-C., Gonzalez, R., Goldsmith, E., & Ellis, L. (1989) *J. Biol. Chem. 264*, 18701−18706.
Eck, M. J., Dhe-Paganon, S., Trub, T., Nolte, R. T., & Shoelson, S. E. (1996) *Cell 85*, 695−705.
Ellis, L., Clauser, E., Morgan, D. O., Edery, M., Roth, R. A., & Rutter, W. J. (1986) *Cell 45*, 721−732.
Engl, J., Moule, M., & Yip, C. C. (1994) *Biochem. Biophys. Res. Commun. 201*, 1439−1444.
Feener, E. P., Backer, J. M., King, G. L., Wilden, P. A., Sun, X. J., Kahn, C. R., & White, M. F. (1993) *J. Biol. Chem. 268*, 11256−11264.
Flores-Riveros, J. R., Sibley, E., Kastelic, T., & Lane, M. D. (1989) *J. Biol. Chem. 264*, 21557.
Frattali, A. L., Treadway, J. L., & Pessin, J. E. (1992) *J. Biol. Chem. 267*, 19521−19528.
Hanks, S. K., Quinn, A. M., & Hunter, T. (1988) *Science 241*, 42−52.
Hasselbacher, C. A., Rusinova, E., Waxman, E., Rusinova, R., Kohanski, R. A., Lam, W., Guha, A., Du, J., Lin, T. C., Polikarpov, I., Boys, C. W. G., Nemerson, Y., Konigsberg, W. H., & Ross, J. B. A. (1995) *Biophys. J. 69*, 20−29.
Ho, S. N., Hunt, H. D., Horton, R. M., Pullen, J. K., & Pease, L. R. (1989) *Gene 77*, 51−59.
Hubbard, S. R., Wei, L., Ellis, L., & Hendrickson, W. A. (1994) *Nature 372*, 746−754.
Isakoff, S. J., Yu, Y.-P., Su, Y.-C., Blaikie, P., Yajnik, V., Rose, E., Weidner, K. M., Sacks, M., Margolis, B., & Skolnik, E. Y. (1996) *J. Biol. Chem. 271*, 3959−3962.
Issad,T., Tavare, J. M., & Denton, R. M. (1991) *Biochem. J. 275*, 15−21.
Kaburagi, Y., Momomura, K., Yamamoto-Honda, R., Tobe, K., Tamori, Y., Sakura, H., Akanuma, Y., Yazaki, Y., & Kadowaki, T. (1993) *J. Biol. Chem. 268*, 16610−16622.
Knighton, D. R., Zheng, J. H., Ten Eyck, L. F., Xuong, N.-H., Taylor, S. S., & Sowadski, J. M. (1991) *Science 253*, 414−420.
Kohanski, R. A. (1989) *J. Biol. Chem. 264*, 20984−20991.
Kohanski, R. A. (1993a) *Biochemistry 32*, 5766−5772.
Kohanski, R. A. (1993b) *Biochemistry 32*, 5773−5780.
Kohanski, R. A., & Schenker, E. (1991) *Biochemistry 30*, 2406−2414.
Mohammadi, M., Schlessinger, J., & Hubbard, S. R. (1996) *Cell 86*, 577−587.
Morrison, B. D., Felz, S. M., & Pessin, J. E. (1989) *J. Biol. Chem. 264*, 9994−10001.
Murakami, M. S., & Rosen, O. R. (1991) *J. Biol. Chem. 266*, 22653−22660.
Palmer, J. L., & Avruch, J. (1981) *Anal. Biochem. 116*, 372−373.
Poon, B., Dixon, D., Ellis, L., Roth, R. A., Rutter, W. J., & Wang, L.-H. (1991) *Proc. Natl. Acad. Sci. U.S.A. 88*, 877−881.
Rajagopalan, M., Neidigh, J. L., & McClain, D. A. (1991) *J. Biol. Chem. 266*, 23068−23073.
Rosen, O. M., & Lebwohl, D. E. (1988) *FEBS Lett. 231*, 397−401.
Sacks, D. B., & McDonald, J. M. (1988) *J. Biol. Chem. 263*, 2377−2383.
Shoelson, S. E., Boni-Schnetzler, M., Pilch, P. F., & Kahn, C. R. (1991) *Biochemistry 30*, 7740−7746.
Sweet, L. J., Morrison, B. D., Wilden, P. A., & Pessin, J. E. (1987) *J. Biol. Chem. 262*, 16730−16738.
Tavare, J. M., & Denton, R. M. (1988) *Biochem. J. 252*, 607−615.
Tavare, J. M., O'Brien, R. M., Siddle, K., & Denton, R. M. (1988) *Biochem. J. 253*, 783−788.
Taylor, S. S., Zheng, J., Radzio-Andzelm, E., Knighton, D. R., Ten Eyck, L. F., Sowadski, J. M., Herberg, F. W., & Yonemoto, W. M. (1993) *Philos. Trans. R. Soc. London 340*, 315−324.
Tavare, J. M., Clack, B., & Ellis, L. (1991) *J. Biol. Chem. 266*, 1390−1395.
Todhunter, J. A., & Purich, D. L. (1977) *Biochim. Biophys. Acta 485*, 87−94.
Tornqvist, H. E., & Avruch, J. (1988) *J. Biol. Chem. 263*, 4593−4601.
Tornqvist, H. E., Pierce, M. W., Frackelton, A. R., Nemenoff, R. A., & Avruch, J. (1987) *J. Biol. Chem. 262*, 10212−10219.
Tornqvist, H. E., Gunsalus, J. R., Nemenoff, R. A., Frackelton, A. R., Pierce, M. W., & Avruch, J. (1988) *J. Biol. Chem. 263*, 350−359.
van der Greer, P., Hunter, T., & Lindberg, R. A. (1994) *Annu. Rev. Cell Biol. 10*, 251−337.
Villalba, M., Wente, S. R., Russell, D. S., Ahn, J., Reichelderfer, C. F., & Rosen, O. R. (1989) *Proc. Natl. Acad. Sci. U.S.A. 86*, 7848−7852.
Walseth, T. F., & Johnson, R. A. (1979) *Biochim. Biophys. Acta 562*, 11−31.
Waxman, E., Rusinova, E., Hasselbacher, C. A., Schwartz, G. P., Laws, W. R., & Ross, J. B. A. (1993) *Anal. Biochem. 210*, 425−428.
Wei, L., Hubbard, S. R., Hendrickson, W. A., & Ellis, L. (1995) *J. Biol. Chem. 270*, 8122−8130.
White, M. F., & Kahn, C. R. (1994) *J. Biol. Chem. 269*, 1−4.
White, M. F., Livingston, J. N., Backer, J. M., Lauris, V., Dull, T. J., Ullrich, A., & Kahn, C. R. (1988) *Cell 54*, 641−649.
Whittaker, J., Okamoto, A. K., Thys, R., Bell, G. I., Steiner, D. F., & Hofmann, C. A. (1987) *Proc. Natl. Acad. Sci. U.S.A. 84*, 5237−5241.
Wilden, P. A., Morrison, B. D., & Pessin, J. E. (1989a) *Biochemistry 28*, 785−792.
Wilden, P. A., Morrison, B. D., & Pessin, J. E. (1989b) *Endocrinology 124*, 971−979.
Zhang, B., Tavare, J. M., Ellis, L., & Roth, R. A. (1991) *J. Biol. Chem. 266*, 990−996.
Zheng, J., Knighton, D. R., Eyck, L. F. T., Karlsson, R., Xuong, N.-h., Taylor, S. S., & Sadowski, J. M. (1993) *Biochemistry 32*, 2154−2161.

BI970170X